Macromolecules

COMMUNICATION TO THE EDITOR

pubs.acs.org/Macromolecules

Dynamics of Entangled Chains in Polymer Nanocomposites

G. J. Schneider,*,† K. Nusser,*,† L. Willner,† P. Falus,‡ and D. Richter†

†Jülich Centre for Neutron Science and Institute for Complex Systems, Forschungszentrum Jülich GmbH, 52425 Jülich, Germany

‡Institut Laue-Langevin, 6 rue Jules Horowitz, 38000 Grenoble, France

INTRODUCTION

Mixing polymer melts with nanosized particles that offer a huge interacting surface leads to novel materials with sometimes exceptional properties, such as mechanically very strong lightweight materials, improved processability, reduced permeability, decreased rolling resistance in tires, etc.[1] Even though polymer nanocomposites have been extensively investigated, many basic questions concerning the molecular origin of their properties are not solved.

Concerning the polymer dynamics that to a large extent determines the mechanical properties of the nanocomposite, widely different and often conflicting results are reported. Starting with small scale local dynamics in both experiments and simulations, mobility gradients in the direction of the particles were reported.[2−4] On the other hand, also data are found where no influence of the nanoparticle could be observed.[5] These results are also manifest in the observation of gradients for the glass transition temperature.[4,6]

On an intermediate scale, the entropy-driven Rouse dynamics takes place. There most of our knowledge comes from simulations that rather generally appear to show an overall slowing down of the Rouse modes.[7−10] Nevertheless, also the observation of a preferably slowing down of the longest wavelength modes is reported.[11]

On a larger scale polymer melts are entangled leading to laterally confined chain dynamics—the reptation process. There the chain moves preferentially along its own profile—lateral motions are restricted by the entanglements. In the frame of the reptation concept the constraints are modeled by a tube following the coarse-grained chain contour. Chain relaxation is achieved if a chain has left its original tube.[12] Simulations indicate that as a consequence of chain confinement by nanoparticles, the entanglement density is reduced.[14] Recently, under strong confinement in nanoporous materials such an increase of the tube diameter was also observed.[15] On the other hand, also an enhanced entanglement network was reported.[16]

Here, in a nanocomposite with nonattractive interactions we investigate the chain dynamics within the polymer matrix, from the initial Rouse dynamics to entanglement controlled motion. Using neutron spin echo spectroscopy, it is possible to directly observe the single chain dynamic structure factor of a polymer chain in the environment of a nanocomposite. We studied poly(ethylene-*alt*-propylene) (PEP) filled with hydrophobically modified silica particles as a function of filler concentration. The key experimental results are (i) the basic Rouse relaxation rate is unaffected even at high filler concentrations, (ii) the effective lateral confinement size or tube diameter is decreasing with increasing filler concentration, and (iii) the data can be rationalized in terms of a gradual crossover from polymer caused entanglements to "particle entanglements" or chain motion under fixed obstacles.

THEORETICAL BACKGROUND

On intermediate length scales, the dynamics of a polymer chain in the melt to a good approximation can be described in terms of the Rouse model that treats the dynamics of a Gaussian chain in a heat bath including entropic forces originating from the conformational chain entropy. At scales $QR_E \gg 1$, where R_E is the chain end to end distance, the normalized single chain dynamic structure factor S can be written as a function of a scaling variable $u = Q^2\ell^2(Wt)^{1/2}$ combining spatial and temporal scales.[12]

$$S(u) = \int_0^\infty \mathrm{d}s \exp\left[-s - \frac{u}{3\pi}\int_0^\infty \frac{\cos(6xs/u)}{x^2}\left(1-\exp(-x^2)\right)\right] \tag{1}$$

There $W = 3k_BT/(\zeta\ell^2)$ is the elementary Rouse frequency. It is given by the ratio of the entropic force $3k_BT/\ell^2$ and the friction coefficient ζ. ℓ^2 is the mean-squared segment length.

At observation times and spatial scales beyond the Rouse regime entanglements lead to a retardation of the structure factor decay—long chains are confined by their mutual entanglements. In the reptation model this lateral confinement is captured by a tube of diameter d following the chain profile. To a good approximation, the coherent dynamic structure factor $S(Q,t)$ takes on the form

$$\frac{S(Q,t)}{S(Q)} = \left(1-\exp\left(-\frac{Q^2d^2}{36}\right)\right)S^{\mathrm{loc}}(Q,t) + \exp\left(-\frac{Q^2d^2}{36}\right)S^{\mathrm{esc}}(Q,t) \tag{2}$$

where $S^{\mathrm{loc}}(Q,t)$ and $S^{\mathrm{esc}}(Q,t)$ are contributions from local Rouse motion along the tube (local reptation) and escape from the tube, respectively[12] (for a more exact implementation of the tube model see also ref 13). In the NSE time window the chains do not yet escape from the tube ($t \ll$ the longest Rouse relaxation time $\tau_R = 1.85 \times 10^4$ ns); therefore, $S^{\mathrm{esc}}(Q,t) = 1$ and the value of d determines the plateau levels. The contribution of the local

Received: April 19, 2011
Revised: June 9, 2011
Published: July 06, 2011

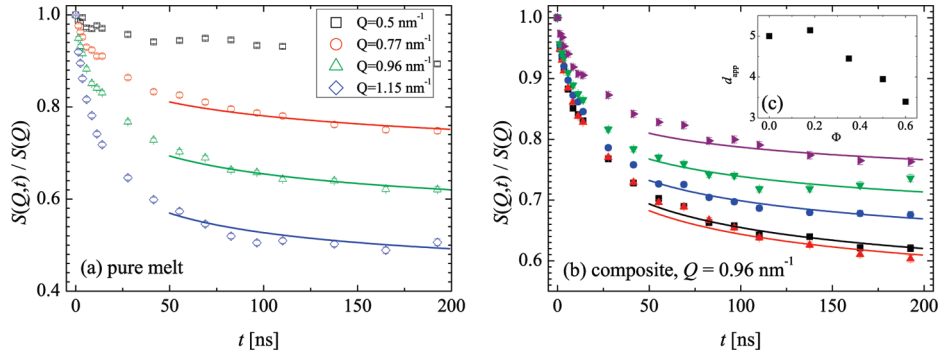

Figure 1. Dynamic structure factor of PEP at various nanofiller volume fractions Φ at $T = 423$ K. (a) Result from a bulk melt (□, $Q = 0.5$ nm^{-1}; ○, $Q = 0.77$ nm^{-1}; △, $Q = 0.96$ nm^{-1}; and ◇, $Q = 1.15$ nm^{-1}). The solid lines display the prediction of eq 2 for long times. (b) Results for filler volume fractions $0 \leq \Phi \leq 0.6$ at $Q = 0.96$ nm^{-1} (□, △, ●, ▽, and tilted △ represent $\Phi = 0$, 0.18, 0.35, 0.50, and 0.6, respectively). Solid lines are fits with eq 2 in the long time regime. (c) Resulting apparent confinement length d_{app}[nm] (Φ).

reptation process in our observation window is given by $S^{loc}(Q,t) = \exp[(t/\tau_0)\ \mathrm{erfc}((t/\tau_0)^{1/2})]$, where $\tau_0 = 36/(W\ell^4Q^4$ is the time scale for the Rouse motion along the tube. Additional confinement that is imposed by the filler nanospheres will add to the tube confinement and lead to an apparently narrower tube.

EXPERIMENTAL SECTION

The experiments were performed on a model system comprising hydrogenated 1,4-polyisoprene chains that were anionically synthesized and Nissan ORGANOSILICASOL Tol-St silica particles at volume fractions $0 \leq \Phi \leq 0.6$. The deuterated and protonated alternating poly(ethylene−propylene) (PEP) chains had a molecular weight of 50 kg/mol with a molecular weight distribution $M_w/M_n = 1.02$. Following ref 17, the Nissan particles have a diameter of $D_{av} = 2R_{av} = 17.0 \pm 0.2$ nm, and the size distribution follows a log-normal distribution $1/((2\pi)^{1/2}\sigma R)\ \exp(-\ln(R/R_{av})^2/(2\sigma)^2)$ with $\sigma = 0.32 \pm 0.02$. We note that D_{av} is significantly larger than the PEP tube diameter (≈ 5 nm). The particle surface is coated with short hydrocarbons making them hydrophobic.

A detailed description of the sample materials and a thorough structural characterization were presented earlier.[17] Therein, in a first series of small-angle neutron scattering experiments (SANS) via contrast variation the scattering length density of the particles was determined to $\rho_p = 2.95 \times 10^{10}$ cm^{-2}. Moreover, the silica showed to be well-dispersed at small and intermediate volume fractions with some signs of clustering at high volume fractions $\Phi \geq 0.35$. Because of the hydrophobic coating, a core−shell structure results that cannot be fully matched. Nevertheless, in the Q range of the dynamic experiments the resulting scattering from the shell does not contribute. Best contrast match was achieved for a mixture of H/D PEP of 52/48 by volume.[17] Because of the high fraction of protonated polymer, the incoherent signal is not negligible. Therefore, in the NSE data analysis of this paper the incoherent dynamic structure factor for reptation was included.[12] The chain conformation in all samples is Gaussian, characterized by a Q^{-2} dependence at high Q. The radius of gyration R_g decreases slightly at high filler fractions Φ.[17]

The dynamic experiments were performed at the neutron spin echo (NSE) instrument IN15 at the Institut Laue Langevin in Grenoble at a temperature $T = 423$ K. We covered a Q range of $0.5 \leq Q \leq 1.15$ nm^{-1} at 423 K for times 100 ps < t < 200 ns using two wavelengths $\lambda = 8$ and 16.8 Å.

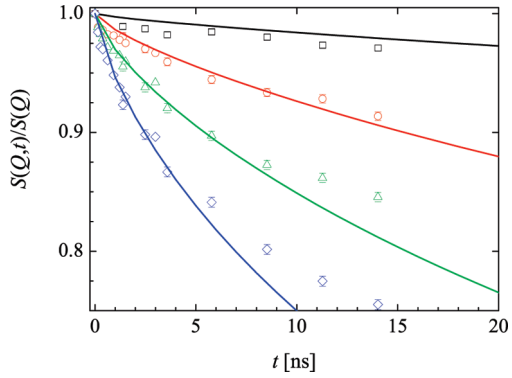

Figure 2. Initial decay of $S(Q,t)$ at $T = 423$ K at $\Phi = 0.35$ for various momentum transfers (□, $Q = 0.5$ nm^{-1}; ○, $Q = 0.77$ nm^{-1}; △, $Q = 0.96$ nm^{-1}; ◇, $Q = 1.15$ nm^{-1}). The solid lines represent a fit with the Rouse structure factor (eq 1) at the initial decay of the bulk result ($W\ell^4 = 0.95$ nm^4/ns).

RESULTS AND DISCUSSION

Figure 1a displays the dynamic structure factor from the reference bulk material. The solid lines indicate the results of a fit with eq 2 in the asymptotic plateau regime. From this fit, we find a tube diameter of 5 nm. This can be compared to an earlier result of $d = 6$ nm that was taken at 492 K. This difference of 17% is consistent with earlier results, where the tube diameter was found to decrease by 16% in changing the temperature from 492 to 423 K.[18,19]

For various filler volume fractions, Figure 1b presents results for the dynamic structure factor at $Q = 0.96$ nm^{-1}. While the data at 0 and 18% filler content are very similar, at higher volume fractions a significant increase of the structure factor at long times is found. The increasing plateau level directly signifies an increase of the apparent confinement for chain motion. For each filler volume fraction Φ four different Q values were studied. In each case a joint fit with eq 2 led to an apparent tube size d_{app} that decreases with increasing Φ. Figure 1c displays the result. From $d_{app}(\Phi = 0) = 5$ nm the tube size decreases with increasing Φ to $d_{app}(\Phi = 0.6) = 3.4$ nm. We note that the Q-dependent sequence of the plateau levels for all Φ is well described by eq 2 (not shown). This indicates that the distribution of the total confinement is well described by a Gaussian distribution.

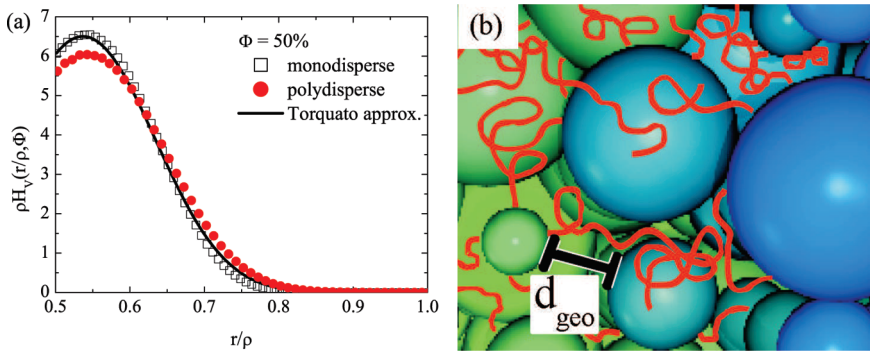

Figure 3. (a) Void distance distribution function within a randomly distributed ensemble of hard spheres at $\Phi = 0.5$. Solid line analytic approximation for the monodisperse system (sphere diameter ρ). □, Simulation for the same system; ○, simulation for a polydisperse system with the characteristics of the nanoparticles. (b) Visualization of the simulated polydisperse particle structure. In the picture polymer chains and the average confinement length d_{geo} according to eq 4 are depicted schematically.

Analyzing the data, we first focus on the short time dynamics that should reflect the underlying Rouse motion of the chains. Figure 2 presents a comparison between the measured structure factor at $\Phi = 0.35$ with that from the bulk sample. The solid lines represent a fit to the initial decay of the bulk spectra with eq 1. We note that—even at high particle concentration—$S(Q,t)$ in its initial part completely agrees with the bulk data. Thus, the initial Rouse motion is unaffected. At $\Phi = 0.35$ as for all other filler concentrations the segmental motion is well described in terms of an undisturbed Rouse model, a finding that agrees with rheological results by Tuteja.[20] Thus, for our sample that is characterized by nonattractive interaction between the hydrocarbons at the filler surface and the hydrocarbon polymer chain we do not find a general slowing down of the Rouse modes nor there exists evidence for a gradient of mobility of any importance in the neighborhood of the filler particles—all segments appear to be equally mobile. For completeness, it should be mentioned, however, that changes out of the time and length scale window of observation are not excluded. This is particularly true for very small distances from the particle surface on the order of one Kuhn segment, where some simulations find an attractive basin even in an otherwise nonattractive situation.[21]

We now interpret the results on the confinement. Let us first summarize the experimental facts: (i) Up to high Φ the chains exhibit a Gaussian conformation. (ii) The local segmental dynamics is unchanged. (iii) All segments are equally mobile. (iv) The apparent confinement length d_{app} decreases significantly with increasing Φ.

The task is now to understand the extra confinement that manifests itself in the decrease of d_{app}. For that purpose we have calculated the nearest-neighbor distance distribution function $\rho H_V(r/\rho,\Phi)$ within the voids of a polydisperse ensemble of spheres at a given volume fraction Φ, where ρ is the average particle diameter. Thereby, $H_V(r,\Phi)$ is the probability that at an arbitrary point in the system the center of the nearest particle lies at a distance between r and $r + dr$. Torquato et al.[22] have given analytical approximations for randomly distributed monodisperse spheres that agree very well with their simulated counterparts. In order to extend to our polydisperse system, we have simulated $H_V(r,\Phi)$ also for a polydisperse particle distribution with a log-normal size distribution characteristic for our ensemble. The simulated situation is visualized in Figure 3b.

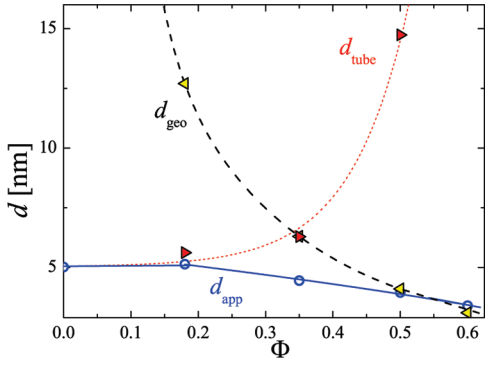

Figure 4. Characteristic confinement lengths in the PEP−nanoparticle system: d_{app} = apparent confinement length from the NSE measurements; d_{geo} = calculated geometrical confinement length; d_{tube} = topological tube confinement according to eq 5.

Figure 3 compares the results for the scaled probability $H_V(r/\rho,\Phi)$ for a monodisperse and polydisperse system. As a solid line also the analytical approximation for the monodisperse system is included. As expected, for the polydisperse case we realize a smearing of the distribution function to larger distances.

With $H_V(r/\rho,\Phi)$ we now may calculate the average mean square distance of a polymer segment from the next neighboring sphere surface:

$$\langle x_{av}^2(\Phi)\rangle = \int_{0.5}^{\infty} \rho H_V(x,\Phi)(x-0.5)^2\, dx \qquad (3)$$

where $x = r/\rho$. In analogy to the tube diameter we define a geometrical confinement length

$$d_{geo}^2(\Phi) = \rho^2\langle x_{av}^2(\Phi)\rangle \qquad (4)$$

Figure 4 presents the volume fraction dependence of d_{geo}. With increasing Φ the geometrical confinement strongly gains importance; e.g. at $\Phi = 50$ vol % $d_{geo} = 4.0$ nm, a value smaller than the tube diameter in the undisturbed melt.

Having measured the apparent confinement length d_{app} and calculated the geometrical confinement length d_{geo}, in a mean field approach we now may calculate the tube diameter d_{tube} that originates from the capacity of the chains to entangle. As the total confinement is well described by a Gaussian distribution of confinement lengths we assume that this holds also for the

dx.doi.org/10.1021/ma200899y |*Macromolecules* 2011, 44, 5857–5860

individual contributions. Then the squares of the individual contributions add inversely:

$$\frac{1}{d_{app}^2(\Phi)} = \frac{1}{d_{tube}^2(\Phi)} + \frac{1}{d_{geo}^2(\Phi)} \quad (5)$$

Following eq 5, d_{tube} as a function of volume fraction may be evaluated. Together with the measured values for d_{app}, the result is included in Figure 4. Seemingly the tube constraints on the chain motion change from polymer entanglements to constraints imposed by fixed obstacles ("particle entanglements"). While at low Φ the polymer imposed entanglements dominate, around $\Phi = 35\%$ both are of similar magnitude. For larger Φ constraints by fixed obstacles prevail. Seemingly, at high Φ, the polymers disentangle completely, and as in de Gennes early reptation approach, the polymer motion is completely constrained by geomatrical hindrance.

Finally, the conclusions from equation eq 5 are the results of a mean field picture that has limited validity, since the relevant length scales d_{tube} and D_{av} are only separated by a factor of 3−4. However, it is useful to gain a first basic understanding of the situation. For a more quantitative evaluation of the situation sophisticated simulations, e.g., with a slip-link approach, would be desirable. Nevertheless, we note that the chain rheology (e.g., the position of the terminal peak) under particle confinement can be quantitatively described with the here extracted mean field parameters (to be published).

CONCLUSION

In this work we have presented a measurement of the polymer chain confinement length on the molecular scale. The increasing plateau levels of the dynamic structure factor at long times, which are observed with increasing filler volume fraction Φ, demonstrate unequivocally the reduction of the confinement length with Φ. Analyzing the geometrical confinement provided by the nanoparticles, we realize that the reduction of the measured confinement length d_{app} is the result of a transition from polymer caused entanglement constraints to chain motion in the presence of fixed obstacles.

Even more, strong evidence for chain disentanglement at high particle fractions was found and, using a mean field approach, quantified by an increase of the respective confinement length d_{tube}. In principle, two possible mechanisms may lead to this disentanglement effect. First, in a nanocomposite a high amount of particle surface is provided. Disentanglement in the vicinity of nonattractive surfaces has been reported in many simulations and could contribute to the observed effect. Second, there may be an additional contribution which arises from the confinement. This kind of disentanglement scenario has been found in the simulation literature for chains confined between smooth nonattractive walls[14] and was also observed experimentally for polymers confined in cylindrical nanopores.[15] It will be a task of the future to distinguish between disentanglement due to the presence of large surface areas in comparison with disentanglement by chain confinement.

Other than in most simulations the experiments do not indicate a general slowing down of the Rouse modes—at least the basic segmental relaxation dynamics is not altered by the presence of fillers, though a particular slowing down of long wavelength Rouse modes as suggested by compliance experiments on nanometer films[23] cannot be excluded, since the signature of such Rouse modes would be overshadowed by confinement effects.

AUTHOR INFORMATION

Corresponding Author

*E-mail: g.j.schneider@fz-juelich.de (G.J.S.); k.nusser@fz-juelich.de (K.N.).

ACKNOWLEDGMENT

We thank Martin Brodeck, Forschungszentrum Jülich, for providing the void distributions of polydisperse spheres. K.N. is grateful for the financial support by the Evonik Stiftung.

REFERENCES

(1) Mai, Y.-W., Yu, Z.-Z., Eds.; *Polymer Nanocomposites*; Woodhead Publishing Ltd.: Cambridge, 2006.
(2) Liu, J.; Cao, D.; Zhang, L.; Wang, W. *Macromolecules* **2009**, *42*, 2831.
(3) Starr, F. W.; Schrøder, T. B.; Glotzer, S. C. *Macromolecules* **2002**, *35*, 4481.
(4) Montes, H.; Lequeux, F.; Berriot, J. *Macromolecules* **2003**, *36*, 8107.
(5) Bogoslovov, R. B.; Roland, C. M.; Ellis, A. R.; Randall, A. M.; Robertson, C. G. *Macromolecules* **2008**, *41*, 1289.
(6) Kalogeras, I. M.; Neagu, E. R. *Eur. Phys. J. E* **2004**, *14*, 193.
(7) Dionne, P. J.; Ozisik, R.; Picu, C. R. *Macromolecules* **2005**, *38*, 9351.
(8) Li, Y.; Wei, D.; Han, C. C.; Liao, Q. *J. Chem. Phys.* **2007**, *126*, 204907.
(9) Picu, R. C.; Rakshit, A. *J. Chem. Phys.* **2007**, *126*, 144909.
(10) Smith, G. D.; Bedrov, D.; Li, L.; Byutner, O. *J. Chem. Phys.* **2002**, *117*, 9478.
(11) Hagita, K.; Ishizuka, D.; Takano, H. *J. Phys. Soc. Jpn.* **2001**, *70*, 2897.
(12) Richter, D.; Monkenbusch, M.; Arbe, A.; Colmenero, J. *Adv. Polym. Sci.* **2005**, *174*, 1.
(13) Likhtman, A. E. *Macromolecules* **2005**, *38*, 6128.
(14) Meyer, H.; Kreer, T.; Cavallo, A.; Wittmer, J. P.; Baschnagel, J. *Eur. Phys. J.: Spec. Top.* **2007**, *141*, 167.
(15) Martin, J.; Krutyeva, M.; Monkenbusch, M.; Arbe, A.; Allgaier, J.; Radulescu, A.; Falus, P.; Maiz, J.; Mijangos, C.; Colmenero, J.; et al. *Phys. Rev. Lett.* **2010**, *104*, 197801.
(16) Riggleman, R. A.; Toepperwein, G.; Papakonstantopoulos, J.; Barrat, J.-L.; de Pablo, J. J. *J. Chem. Phys.* **2009**, *130*, 244903.
(17) Nusser, K.; Neueder, S.; Schneider, G. J.; Meyer, M.; Pyckhout-Hintzen, W.; Willner, L.; Radulescu, A.; Richter, D. *Macromolecules* **2010**, *43*, 9837–9847.
(18) Richter, D.; Farago, B.; Butera, R.; Fetters, L. J.; Huang, J. S.; Ewen, B. *Macromolecules* **1993**, *26*, 795.
(19) Wischnewski, A.; Monkenbusch, M.; Willner, L.; Richter, D.; Kali, G. *Phys. Rev. Lett.* **2003**, *90*, 058302.
(20) Tuteja, A.; Mackay, M. E.; Hawker, C. J.; van Horn, B. *Macromolecules* **2005**, *38*, 8000.
(21) Alexander-Katz, A.; Moreira, A. G.; Fredrickson, G. H. *J. Chem. Phys.* **2003**, *118*, 9030.
(22) Torquato, S.; Lu, B.; Rubinstein, J. *Phys. Rev. A* **1990**, *41*, 2059.
(23) O'Connell, P. A.; McKenna, G. B. *Eur. Phys. J. E* **2006**, *20*, 143.
(24) Lu, B.; Torquato, S. *Phys. Rev. A* **1992**, *45*, 5530.